

Percolation superconductivity in $\text{La}_2\text{CuO}_{4.06}$ by imaging bulk lattice granularity using scanning micro-XANES

Nicola Poccia^{1,2}, Matthieu Chorro³, Alessandro Ricci^{4,2}, Wei Xu⁵, Augusto Marcelli^{6,7,2}, Gaetano Campi^{8,2} and Antonio Bianconi^{2,8}

¹ MESA+ Institute for Nanotechnology, University of Twente, P. O. Box 217, 7500AE Enschede, Netherlands.

² RICMASS Rome International Center for Materials Science Superstripes, via dei Sabelli 119A, 00185 Roma, Italy.

³ Synchrotron SOLEIL L'Orme des Merisiers, 91190 Paris S.Aubin, France.

⁴ Deutsches Elektronen-Synchrotron DESY, Notkestraße 85, D-22607 Hamburg, Germany

⁵ Beijing Synchrotron Radiation Facility, Institute of High Energy Physics, Chinese Academy of Sciences, 100049, P. R. China

⁶ Istituto Nazionale di Fisica Nucleare - Laboratori Nazionali di Frascati, 00044 Frascati, Rome, Italy

⁷ NSRL, University of Science and Technology of China, Hefei, 230026, P.R. China

⁸ Institute of Crystallography, CNR, via Salaria Km 29.300, Monterotondo, 00015 Rome, Italy.

Abstract

The simplest cuprate superconductors $\text{La}_2\text{CuO}_{4+y}$ (LCO) was known to show phase separation, but the bulk spatial distribution of oxygen rich domains has been measured only recently by using scanning micro x-ray diffraction. The spatial distribution of superconducting units is a key parameter controlling percolation superconductivity in layered perovskites. These oxides form supra-molecular architectures called heterostructures at atomic limit made of superconducting atomic monolayers intercalated by spacers made of molecular blocks. Oxygen interstitials (Oi) enter into the rocksalt $\text{La}_2\text{O}_{2+y}$ spacer layers forming “Oi rich puddles” (ORP) and “Oi poor puddles” (OPP). The spatial distribution of the puddles has been determined here by using scanning micro X-ray absorption near edge structure (S μ XANES) at the La LIII-edge XANES. Percolating networks of ORP or percolating networks of OPP puddles are observed in different micrometer portions of the crystals providing evidence for the superstripes scenario. The complex surface resistivity shows two superconducting critical temperatures associated with the complex percolation superconductivity in this granular matter. The similarity of oxygen doped LCO with the well established phase separation in iron selenide superconductors is discussed.

Keywords: superstripes, X-ray absorption, defects, cuprates, oxygen interstitials, puddles, disorder, phase separation

Introduction

Complex lattice architectures composed of transition metal oxides can display a rich variety of nanoscale electronic and magnetic phases going from superconductors, multiferroic, and colossal magnetoresistance units [1,2]. A new low energy physics going beyond the standard condensed matter, called soft electronic matter, is emerging and open new perspectives to nano-technology [3]. Understanding these electronic phases, emerging

from nanoscale to micron scale, need the development of new methods where bulk average experimental probes fail to study the competing nano-scale heterogeneous phases.

The study and the control of the spatial organization of defects in transition metal oxides is a key point in this field [5,6]. New insights in this physics can be obtained from experimental probes that provide spatially resolved bulk information; in fact the standard scanning tunneling microscopy provides only information

on the sample surface [7]. In the XX century local structure experimental probes, probing the nanoscale structure, without time or spatial averaging like Pair Distribution Function analysis of neutron diffraction [8,9] or X-ray Absorption Near Edge structure (XANES) [10-15] have been developed. These local methods, applied to complex high T_c superconductors [16-22], have provided evidence for local electronic and lattice fluctuations not observed by diffraction methods. These local atomic-scale lattice fluctuations in the active CuO_2 plane have been shown to favor high temperature superconductivity (HTS) [23,24]

Based on these experiments the superstripes scenario for cuprate superconductors has been proposed (25-29), where nanoscale puddles form superconducting networks in two-dimensional layers embedded in heterostructures at atomic limit. Several theoretical works have supported the experimental findings [30-36]. This emerging scenario is a particular case of percolation superconductivity [37-54].

A similar superconducting phase emerging from percolation of multi-condensates puddles has been recently observed in iron selenide superconductors. Here the scientific agreement has been reached rapidly on the complex structural phase separation in $\text{R}_y\text{Fe}_{2-x}\text{Se}_2$ (with $\text{R}=\text{K}, \text{Rb}, \text{Cs}$) where different magnetic domains and networks of metallic domain walls are essential features for HTS [55-58].

Electronic phase separation in strongly correlated superconductors is predicted by multiband Hubbard models near a Lifshitz transition [59] and complex time dependent phenomena have been observed [60,61].

There is now high interest to control the nanoscale phase separation in strongly correlated materials by controlling lattice modulations and defects multiscale organization. Only recently the distribution of lattice defects in high temperature superconductors (HTS) has been found to play a key role. [62-68]. The defects distribution control the electronic features in the range of 10-100 meV near the Fermi level [69] which is the relevant energy scale to control advanced electronic nano-devices.

Here we have applied scanning micro XANES [70] to investigate the statistical distribution of oxygen interstitials (O_i) in superoxygenated $\text{La}_2\text{CuO}_{4+y}$. This new approach is complementary to scanning micro x-ray diffraction applied to investigate these complex materials [62-66]. In fact X-ray diffraction is a non-local probe of the k-space i.e., it is sensitive only to puddles of

ordered O_i over a scale larger than the diffraction coherence length while XANES is a local probe of the lattice local structure within a nanoscale cluster centered at the selected absorption site. Therefore S_μXANES is a promising tool with both local and spatial sensitivity to investigate complex multiphase materials

$\text{La}_2\text{CuO}_{4+y}$ is a prototype of cuprate superconductors showing phase separation. Early neutron powder diffraction studies have shown the phase separation for $y < 0.055$ [71] and the average location of the oxygen interstitials O_i [72]. Further neutron powder diffraction work [73] has established a phase diagram for $\text{La}_2\text{CuO}_{4+y}$ with $0 < y < 0.055$, demonstrating a miscibility gap between an antiferromagnetic phase at $y \sim 0.01$ and a superconducting phase at $y \sim 0.055$. Phase separator for $y > 0.055$ was object of discussion for a long time. Neutron diffraction on single crystals at higher concentration of oxygen interstitials [74-77] have provided evidence for superstructure satellites, but few information on the spatial location of multiple phases could be extracted. An EXAFS experiment on a $y=0.1$ samples has shown local lattice fluctuations in the CuO_2 plane [78]. The oxygen interstitials have a large mobility in this system since the spacer layers are under a large tensile stress due to lattice misfit between the active and spacer layers [79-82].

Only recently the spatial distribution of puddles with 3D ordered oxygen interstitials (O_i) has been unveiled in the real space by scanning x-ray diffraction in optimal ($T_c = 40$ K) $\text{La}_2\text{CuO}_{4+y}$ superconducting samples [62] and in an underdoped single $\text{La}_2\text{CuO}_{4+y}$ crystal (with $y = 0.06$) [63, 64]. These experiments pointed out that O_i rich puddles (ORP) with the characteristic q_2 - O_i satellites form a network of superconducting puddles with a power law distribution at the optimum doping which favors HTS. Therefore there is need to develop different experimental approaches, probing bulk spatial distribution of local lattice fluctuations.

Here we report an experiment of S_μXANES to provide further information on the local atomic structure of an underdoped $\text{La}_2\text{CuO}_{4+y}$. XANES has been widely used to get structural information on nanoscale local structure with no space or time averaging (being a fast probe with a femtosecond time scale) [12-15]. We have focused on XANES at the Lanthanum LIII-edge [25-29], probing directly the local structure within 0.5 nm around the selected La atomic species in the spacer layer in $\text{La}_2\text{CuO}_{4+y}$.

Materials and Methods

We have examined a $\text{La}_2\text{CuO}_{4+y}$ single crystal, with the space group $Fmmm$, in the underdoped regime with $y = 0.06$, which corresponds to an electronic doping of 0.1 holes per Cu site. The sample was grown first as La_2CuO_4 by the flux method and then it was doped by electrochemical oxidation. Details on sample characterization are presented in ref. 63.

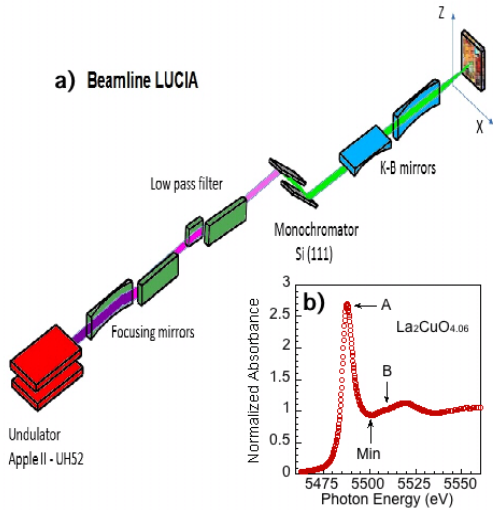


Figure 1. *a)* Experimental setup for the $S\mu\text{XANES}$ measurements, performed on the dedicated-beamline LUCIA at the SOLEIL Synchrotron. The monochromatic X-ray beam is focused on a selected spot of $2.5 \times 2.5 \mu\text{m}^2$. *b)* A typical La LIII-edge XANES spectrum of $\text{La}_2\text{CuO}_{4+y}$ ($y = 0.06$) recorded in fluorescence mode on a single micrometer spot.

The $S\mu\text{XANES}$ measurements were performed on the beamline LUCIA at the SOLEIL Synchrotron [70] shown in Fig. 1 using focused synchrotron radiation beam. The x-ray source is an electron undulator Apple II-UH52, operating in the range of soft X-rays (0.8-8 KeV) with high brilliance ($\sim 1.6 \times 10^{11}$ ph/s/400 mA) equipped with a double Si-111 monochromator. The monochromatic photon beam is focused on a spot of $2.5 \times 2.5 \mu\text{m}^2$ with a Kirkpatrick-Baez mirrors apparatus. The sample is mounted on a x-z translator that allows micrometer step resolution as shown in panel a) of Figure 1. At each spot, the Lanthanum LIII-edge XANES for electronic transition from the core level at 5383 eV binding energy was recorded in fluorescence mode with a 4 element silicon drift Bruker detector. A typical La LIII-edge spectrum is shown in panel b) of Figure 1. The spectrum is very simple showing two multiple

scattering resonances [10-15] A and B separated by a minimum (Min) which are determined by the local structure of a nanoscale cluster of neighbor atoms surrounding the absorbing La ion.

Results and discussion

Using $S\mu\text{XANES}$, we have combined the real space scanning point-to-point and the XANES response, probing the local structure around the La ion in the spacer layers. This is obtained by recording polarized $E//ab$ La LIII-edge XANES spectra at the $\text{La}_2\text{CuO}_{4+y}$ crystal at each $2.5 \times 2.5 \mu\text{m}^2$ illuminated spot. The La LIII-XANES spectra were recorded with energy steps of 0.2 eV in the near edge region and 4 s integration shown in Fig. 2. We have found that the XANES spectra collected in different spots are different from spot to spot. Figure 2 (upper panel) shows two typical La LIII-edge XANES spectra, collected in two different spots of the sample.

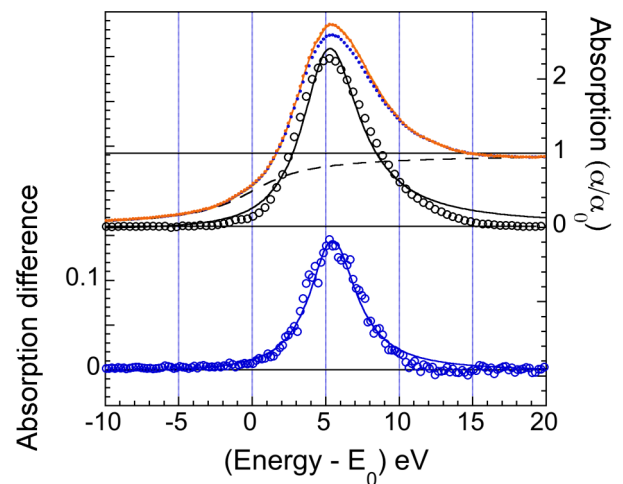


Figure 2. **Upper panel** Two typical La LIII edge XANES spectra (blue and red dots) recorded at two different illuminated spots of the same crystal. The black dashed line is the atomic absorption. The difference between the experimental absorption and the atomic absorption is shown by the empty black circles in the upper panel. This curve is the measure of the partial absorption cross section for final states where the photoelectron is trapped in a nanoscale cluster for a finite time in a shape resonance [10-15]. The black continuous curve is the fit of the shape resonance by a Fano lineshape curve. **Lower panel.** The difference of the XANES spectra recorded in two different spots (i.e., at two 2.5×2.5 microns pixels) of the sample. The experimental difference is well beyond the error bar and it is like the shape resonance. The XANES difference from point to point in the real space lower panel is determined by the variation of the shape resonance from point to point.

The typical spatial variation of the La LIII-edge XANES spectra is shown by the XANES difference spectrum shown in the lower part of Fig. 2. Where the difference spectrum shows only a broad peak centered at 5 eV above the ionization threshold well above the noise level.

The XANES spectra of condensed matter [10-15] are determined by core excitons below the atomic ionization threshold and shape resonances above the absorption threshold. The typical $E//ab$ polarized La LIII-edge XANES spectrum shown in Figure 2 is very simple since no bound excitons are appear below the absorption threshold to continuum. The absorption spectrum above threshold is given by

$$\alpha(\omega) = \alpha_a(\omega)[1 + \chi(\omega)] = \alpha_a(\omega) + \alpha_a(\omega)\chi(\omega)$$

where $\alpha_a(\omega)$ is the atomic absorption due to electronic transitions from the isolated Lanthanum ion to the continuum and $\chi(\omega)$ is the modulation of the atomic absorption cross section from the atomic La $(2p)_{3/2}$ core level to photoelectron final states degenerate with the continuum. The local lattice structure controls the photoelectron final states and therefore controls $\chi(\omega)\alpha_a(\omega)$.

$\chi(\omega)\alpha_a(\omega)$ shown in Figure 2 has been easily extracted by subtracting the atomic absorption from the experimental spectrum. The atomic absorption spectrum has been easily obtained by fitting the experimental XANES spectrum with an arctangent in a range of 10 eV below the absorption edge and in the range between 15 and 20 eV above the absorption edge as it is shown in Figure 2. The inflection point at E_0 of the arctangent line has been selected as the zero of the energy scale. E_0 is the ionization potential of the La $(2p)_{3/2}$ core level and therefore is the energy threshold for electronic transition to the continuum. The measured absorption coefficient α has been divided by the value of the atomic absorption spectrum at high energy α_0 . Therefore α/α_0 is the absorption coefficient measured in units of the atomic X-ray absorption jump at the La LIII-edge

The extracted modulation factor $\chi(\omega)\alpha_a(\omega) = \alpha(\omega) - \alpha_0(\omega)$ contains structural information is shown in the upper panel in Figure 2. This spectrum shows a single broad asymmetric peak centered at energy 5 eV. This broad peak is clearly a shape resonance [11,12] which is due a quasi bound state of the excited photoelectron confined in a nanoscale cluster [10-15]. This quasi bound state arises by a multiple scattering resonance (MSR). The configuration interaction between the MSR quasi bound state and the continuum is expected to give a spectral Fano

lineshape. Therefore the Fano lineshape is a fundamental feature of MSR in XANES spectra [10-15]. This interpretation is confirmed by the good fit with a Fano lineshape of the MSR, shown in the upper part of Figure 2.

The lower panel in Figure 2 shows that the difference of the two XANES spectra recorded in different points shows a similar Fano lineshape as the shape resonance in the upper panel. It is well established that α_0 being the atomic cross section should not show any spatial dependence [10-15], therefore the difference between the two XANES spectra shown in the lower panel of Figure 2 is due to $\alpha_2(\omega) - \alpha_1(\omega) = \alpha_a(\omega)\chi_1(\omega) - \alpha_a(\omega)\chi_2(\omega)$ which is determined by the difference of the multiple scattering resonance (MSR) changing from spot to spot. Therefore the raw data of the difference XANES spectra clearly indicate a relevant spatial variation of the local structure: the cluster of neighbor atoms surrounding the absorbing La atom.

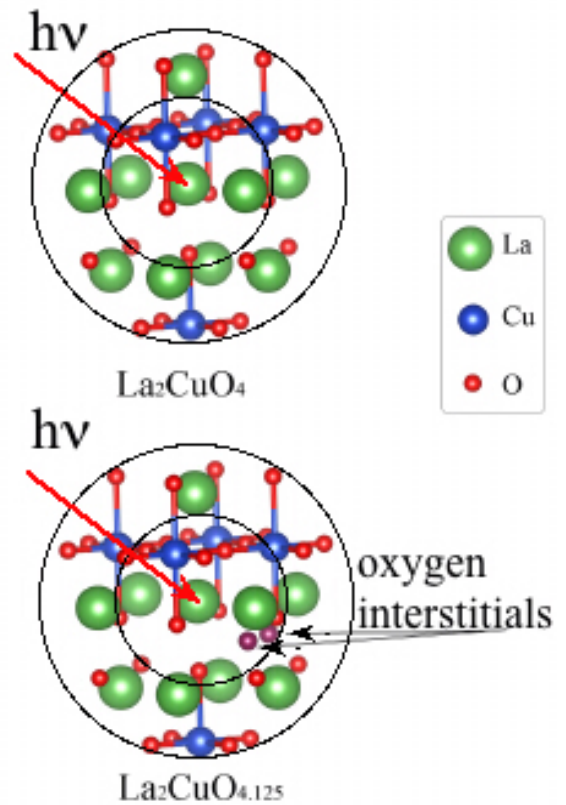


Figure 3. The cluster of neighboring atoms surrounding the La absorbing atom (green sphere, indicated by the red arrow) in a $\text{La}_2\text{CuO}_{4+y}$ crystal that determines the shape resonance in the La LIII XANES. The black circles provide a pictorial view of the photoelectron wave emitted by the absorbing atoms, scattered by neighboring atoms Cu (blue sphere) and oxygen (red sphere) and La ions. The size of the cluster is 8 Å. In oxygen rich puddles (like in the local structure of the $\text{La}_2\text{CuO}_{4.125}$ crystal) the cluster includes three additional oxygen interstitials (indicated by the black arrows).

strongest MSR as shown in the lower panel of Fig. 4.

The determination of the size of the nanoscale cluster probed by the excited photoelectron in the XANES spectra is the first step for its quantitative interpretation. The size of the cluster depends on many body excitations controlling the mean free path of the excited photoelectron inside the material and the core hole lifetime. The lifetime of the final state is in the femtosecond range therefore the final states probe the structure of the nano-cluster.

The Lanthanum L_3 edge XANES is determined by dipole transitions from the $La(2p_{3/2})$ initial state ($n=2, L=1, J=3/2$) of the photon-absorbing La atom in the spacer layers $La_2O_{2.06}$ to final states consisting of multiple scattering resonances of the emitted photoelectron with $L=2$ orbital moment.

The La LIII-XANES spectra were calculated using full multiple scattering theory based on self-consistent-field potential with muffin-tin approximation, as implemented in the FEFF9.0 code. The original $Fmmm$ La_2CuO_4 is used to simulate the size of the cluster that is needed to reproduce all experimental XANES spectrum. The SCF radius is 5 Å and the full multiple scattering radius is 8 Å, which is sufficient to achieve good convergence. The Hedin-Lundqvist exchange-correlation potential is used. We have found that the cluster probed by La LIII-edge XANES, shown in Figure 3, is made of 21 moles of La_2CuO_4 with a radius of 0.8 nm.

From previous micro X-ray diffraction experiments [62,63], we know that in our sample there are first, nanoscale oxygen interstitials (Oi) poor puddles (OPP) with stoichiometric oxygen content and second nanoscale Oi rich puddles (ORP) with oxygen formal content 4.125 revealed by a commensurate superstructure satellite.

The calculations for the expected XANES spectrum for OPP have been carried out using a cluster model like in $Fmmm$ La_2CuO_4 and the XANES spectrum for ORP has been calculated using the local structure of doped $La_2CuO_{4.125}$.

To account for the ORPs with Oi located in the $1/4, 1/4, 1/4$ site, and forming compositional stripes in the La_2O_2 structure, we have to include three Oi in the atomic cluster probed by the photoabsorption final state around La absorbing atom in the spacer La_2O_2 layers as shown in Fig. 3.

The results of our calculations are shown in Fig. 4. The presence of Oi induces an increase of the peak A (peak A in Figure 1) due to the first and

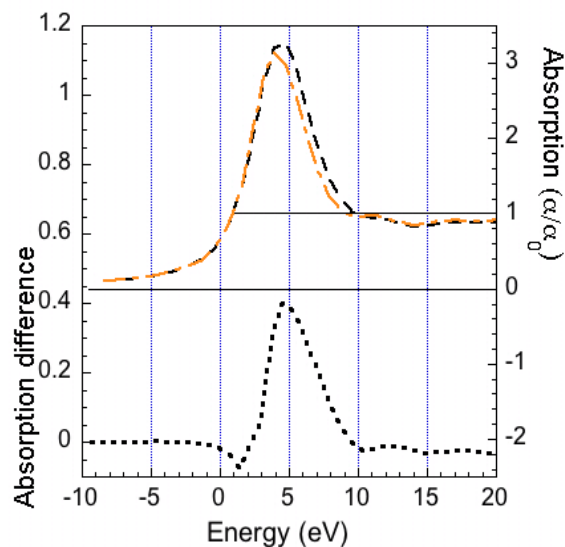


Figure 4. Upper panel. XANES computer code calculation of the La LIII absorption edge, using the size of the cluster shown in Figure 3 for La_2CuO_4 (brown dashed line) and $La_2CuO_{4.125}$ (black dashed line). Lower panel. It shows the absorption difference between the two spectra.

Figure 4, upper panel, shows the superimposition of two XANES spectra in the ORPs i.e., like in La_2CuO_{4+y} with $y = 0.125$ Oi, and in the OPPs, i.e., like La_2CuO_4 without oxygen interstitials ($y = 0$), computed through XANES Full Multiple Scattering theory. The graph shows the increasing intensity of peak A by 0.4 in units of the La LIII-edge atomic absorption jump and a slight shift in the white-line peak in correspondence of the oxygen rich puddles. The calculation has been done using the size of the cluster, as shown in Fig. 3, both for the La LIII-edge XANES spectrum of the $La_2CuO_{4.125}$ cluster and the La LIII-edge XANES spectrum of the La_2CuO_4 cluster.

Figure 4, lower panel, shows the difference between the two spectra. Given that the atomic component is removed in the difference spectrum the presence of the additional oxygen interstitials in proximity of the La absorbing atom clearly indicates an increase of the MSR at 5 eV above threshold.

The XANES spectrum recorded over a micron size spot is already the averaged ratio between ORP and OPP nanoscale puddles in the same micron size illuminated spot. Our underdoped sample ($y = 0.06$) will present a content of Oi intermediate between the La_2CuO_4 and the optimally doped $La_2CuO_{4.125}$ samples, which we

considered for calculations.

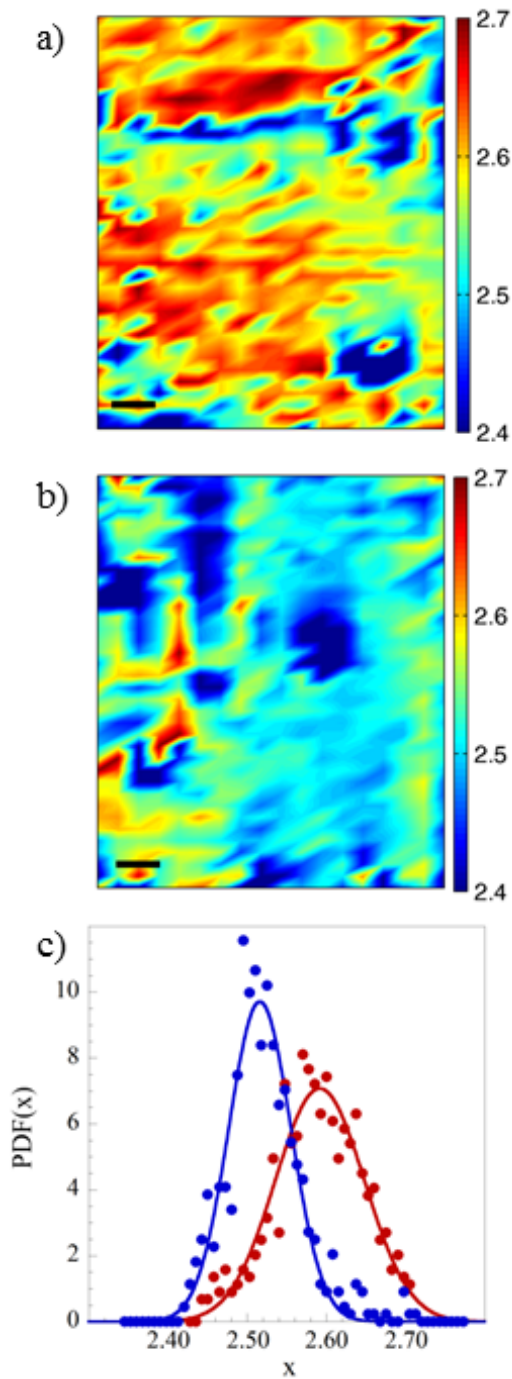


Figure 5. **a, b** Colormaps of the position dependent intensity of the multiple scattering resonance in the XANES spectra, of the investigated $\text{La}_2\text{CuO}_{4.06}$ crystal (the scale of intensity is depicted in the colorbar next to the map). The maps are a 36×18 pixels ($4 \mu\text{m}$ pixel size). The black bar corresponds to 10 microns. The exposition time is 10 s/step. **c** It shows the probability density function $\text{PDF}(x)$ of the multiple scattering resonance for the two region of interest.

Having established the relation between the variation of the main MSR peak of our XANES spectra and the presence of Oi in the illuminated

spots we have measured the variation of the intensity of the main MSR peak in the XANES spectra using the focused X-ray beam with motor step of $4 \mu\text{m}$. The distribution of ORP and OPPs is revealed by the map of the space variation of the MSR, peak A, in Figure 5. We show in Fig. 5 the images of two regions with different distributions of ORPs.

The statistical analysis of the two regions of the sample is shown in Fig. 5c. The x axis in figure 5c is the intensity of the MSR, which ranges from 2.4 to 2.7 in units of the La LIII-edge absorption jump. The distribution measured for the upper panel (5a) is peaked at 2.6, while the lower panel (5b) is peaked at 2.5. Both regions display a Gaussian distribution. The distribution curves of the color-map in panel 5a (5b) are plotted in panel c with red (blue) color dots. The width of the oxygen poor distribution ranges from 2.45 to 2.55, while in the oxygen rich region ranges from 2.52 to 2.65, showing a substantial variation of the distribution of ORPs in the same crystal, in different spots illuminated by X-ray beam. The variation of the MSR intensity is of 0.3 instead of the calculated value 0.4 since using a micron-scale X-ray beam size it is impossible to completely probe a region without any Oi rich puddle (ORP). This is further supported by nano X-ray diffraction experiments in a similar crystal [63], showing that it is impossible to find a region smaller than 4 microns without ORP.

The results show an intrinsic phase separation in a single crystal of an underdoped $\text{La}_2\text{CuO}_{4+y}$, revealing the coexistence of ORPs and OPPs, characterized respectively by a stronger and weaker MSR peak of the XANES spectra. The maps show two kinds of percolation of ORP in the system. In order to understand the effect on superconductivity, we have measured the complex surface resistivity of the sample, as shown in Fig. 6.

The surface complex resistivity was measured to get the superconducting critical temperature. The single-coil inductance technique, nondestructive and contactless, enables us to measure the complex conductivity of the same crystal surface investigated by X-Ray diffraction. A spiral coil of 0.5 mm diameter with an inductance L , is placed on the sample surface illuminated by x-rays. A change of impedance of the LC circuit is detected as a change of resonant frequency ω , 2–4 MHz, and amplitude V of the oscillating signal. The very high sensitivity of the method arises from the strong mutual inductance between sample and coil in the single-coil geometry. The temperature

variation of the ratio of the resonant frequency and the reference frequency of the coil measured in the proximity of non-superconducting copper metal is a measure of the surface resistivity at frequency, proportional to the London penetration depth.

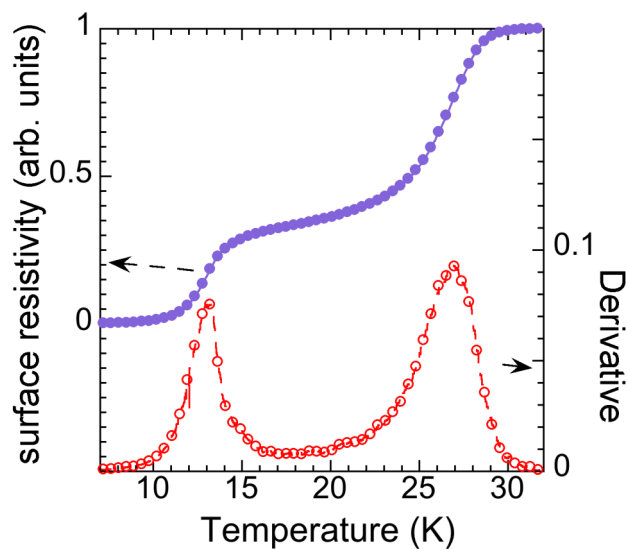


Figure 6. Temperature-dependent complex surface resistivity of the underdoped $\text{La}_2\text{CuO}_{4+y}$ superconducting crystal (blue line) and its derivative (red line) show two critical temperatures $T_{c1}=13$ K and $T_{c2}=27$ K. We used a single-coil inductance method recording $(\omega_0/\omega(T))^2$, where $\omega(T)$ is the resonance frequency of an LC circuit, L is the inductance of the coil placed near the surface of the superconducting sample and ω_0 is the reference resonance frequency for a non-superconducting sample.

The surface resistivity is shown in Figure 6. The results provide evidence for a first jump at T_{c2} 27 K and a second jump at $T_{c1}=13$ K, in agreement with previous experiments [63,83]. While we provide a correlation of these jumps with percolation effects in the networks of nanoscale puddles with the different distributions of ORPs shown in Fig. 5, further works are needed to clarify the details of percolation superconductivity in this complex material.

In conclusion, we have reported scanning μ -XANES investigation for an underdoped cuprate oxide with mobile O_i dopants, showing the complex spatial distribution of ORPs on micron scale spatial images. μ XANES technique is well performing to visualize the nature of multi-scale systems being a fast and local probe of a selected atomic species. These results are complementary to scanning micro X-ray diffraction [62,63], providing further support to the scenario of percolation superconductivity in copper oxides. The arrangement of O_i rich puddles in real space

shows compelling evidence of different percolation regimes occurring in this system. The percolation has a strong influence in the superconducting properties measured as shown by the two critical temperatures supporting theoretical models [30-54] which consider the intrinsic percolative nature of superconductivity.

Acknowledgments

N.P. acknowledge the Marie Curie Intra European Fellowship for financial support. N.P. thanks Hans Hilgenkamp and the ICE group of the University of Twente for useful discussion and support. W.X. acknowledges National Natural Science Foundation of China (Grant No. 11105172). A.B and N.P. acknowledge Superstripes Institute, and European CALIPSO TransNational Access Program of programs of SOLEIL for financial support.

References

1. Mannhart J and Schlom D G 2010 *Science* 327 1607-1611.
2. Kalinin S V, Borisevich A, and Fong D. 2012 *ACS nano* 6, 10423-10437.
3. Littlewood P B, 2012 *Disorder and Strain-Induced Complexity in Functional Materials*. Springer Berlin Heidelberg, 95-112.
4. Kalinin S V and Spaldin N A 2013 *Science* 341 858.
5. Littlewood P B 2011 *Nat. Mater.* 10, 726-727.
6. Poccia N *et al.* 2011 *Nat. Mater.* 10, 733-736.
7. Bryant C, Renner Y, Tokunaga Y., Tokura Y, Aeppli G 2011 *Nat. Comm.* 2, 212.
8. Egami T and Billinge S J L. 2003 *Underneath the Bragg peaks: structural analysis of complex materials*. 16. Elsevier,
9. Billinge S J L and Levin I, 2007 *Science* 316, 561.
10. Bianconi A, Doniach S, Lublin D 1978 *Chem. Phys. Lett.* 59, 121-124.
11. Bianconi A 1980 *App. Surf. Science* 63, 392-418.
12. Bianconi A, Dell'Aricecia M, Durham P, and Pendry J 1982 *Phys. Rev. B* 26, 6502.

13. Garcia J, Bianconi A, Benfatto M, Natoli C R 1986 *Le Journal de Physique Colloques* **47**, C8-49-C8-54.
14. Bianconi A in Koningsberger D C, Prins R (eds) 1988 *X-ray absorption: principles, applications, techniques of EXAFS, SEXAFS and XANES* 573, John Wiley & Sons: New York.
15. Bianconi A, Garcia J, Benfatto M 1988 *Chapter Synchrotron Radiation in Chemistry and Biology I in Topics of Current Chemistry*, 145, 29A.
16. Bianconi A, Congiu Castellano A, De Santis M, Rudolf P, Lagarde P, Flank A M, and Marcelli A, 1987 *Sol. Stat. Comm.* **63**, 1009.
17. Bianconi A *et al.* 1991 *Phys. Rev. B* **44**, 10126-10138.
18. Bianconi A, Della Longa S, Missori M, Pettiti I, and Pompa M, 1992 *Lattice effects in High-Tc superconductors* (Y., Bar-Yam, Egami, T., Leon, J. M., Bishop, A. R. eds) pp. 65-76 (World Scientific Pub., Singapore).
19. Bianconi A *et al.* 1993 *Jpn. J. Appl. Phys.* **32**, 578-580.
20. Bianconi A and Missori M, *Sol. Stat. Comm.* **91**, 287-293 (1994).
21. Missori M, Bianconi A, Oyanagi H and Yamaguchi H 1994 *Phys. C: Supercond.* **235-240**, 1245-1246.
22. Bianconi A *et al.* 1995 *Europhys. Lett.* **31**, 411-415.
23. Bianconi A *et al.* 1996 *Phys. Rev. Lett.* **76**, 3412.
24. Saini N L *et al.* 2012 *J. Appl. Phys.* **111**, 112622.
25. Bianconi A 2000 *Int. J. Mod. Phys. B* **14**, 3289-3297.
26. Bianconi A, Saini N L, Agrestini S, Di Castro D, Bianconi G 2000 *Int. J. Mod. Phys. B* **14**, 3342-3355.
27. Bianconi A *et al.* 2000 *Phys. C: Supercond.* **341-348**, 1719-1722.
28. Bianconi A, Innocenti D, Campi G 2013 *Journal of Superconductivity and Novel Magnetism* **26**, 2585-2588.
29. Bianconi A 2013 *Nat. Phys.* **9**, 536-537.
30. Bishop A R 2008 *J. Phys.: Conf. Ser.* **108**, 012027.
31. Gor'kov L P, and Teitelbaum G B, 2010 *Phys. Rev. B* **82**, 020510.
32. Kresin V, Ovchinnikov Y, and Wolf S, 2006 *Phys. Rep.* **431** 231-259.
33. Phillips J C 2014 *J. Supercond. Nov. Magn.*, **27**, 345-347.
34. M.-Yu Kagan, and K.I. Kugel. 2001 *Phys.-Uspekhi* **44**, 553.
35. Dagotto E 2013 *Rev. Mod. Phys.* **85**, 849.
36. de Mello E V L 2012 *Europhys. Lett.* **98** 57008.
37. Deutscher G *et al.* 1980 *Phys. Rev. B* **21**, 5041-5047.
38. Alexander S 1983, *Phys. Rev. B* **27**, 1541.
39. Alexander S, and Halevi E 1983 *J. de Physique* **44**, 805-817.
40. De Arcangelis L, Redner S, and Coniglio A 1986 *Phys. Rev. B* **34**, 4656.
41. Deutscher G, and Müller K A *Phys. Rev. Lett.* 1987 **59**, 1745-1747.
42. Hizhnyakov V, Kristoffel N, and Sigmund E. 1989 *Phys. C: Supercond.* **160**, 119-123.
43. Kubo Y, and Igarashi H. 1989 *Phys. Rev. B* **39**, 725.
44. Phillips J C, 1989 *Phys. Rev. B* **40**, 8774.
45. Mitsen K V, and Ivanenko O M 2000 *J. Exp. Theo. Phys.* **91**, 579-587.
46. Mihailovic D, Kabanov V V, and Müller K. A 2002 *Europhys. Lett.* **57**, 254.
47. Zeimet B, Glowacki B A, and Evetts J E 2002 *Euro. Phys. J. B-Cond. Matty. Com. Sys.* **29**, 359-367.
48. Frary M, and Schuh C A 2003 *Appl. Phys. Lett.* **83**, 3755-3757.
49. Rutter N A *et al.* 2005 *Appl. Phys. Lett.* **87**, 162507-162507.
50. Yamamoto A *et al.* 2007 *Supercond. Scie. Tech.* **20.7**, 658
51. Strel'niker Y M, Frydman A, and Havlin S 2007 *Phys. Rev. B* **76**, 224528.
52. Bianconi G 2012 *Phys. Rev. E* **85**, 061113.
53. Bianconi G 2012 *J. Stat. Mech.: Theo.*

- Exp.* 2012, P07021+.
54. Bianconi G, 2013 *Europhys. Lett.* 101, 26003.
 55. Ricci A *et al.* 2011 *Phys. Rev. B* 84, 060511.
 56. Ksenofontov V *et al.* 2011 *Phys. Rev. B* 84, 180508.
 57. Shermadini Z *et al.*, 2011 *Phys. Rev. Lett.* 106, 117602.
 58. Eisterer M *et al.* 2010 *Supercond. Scie. Tech.* 23, 054006.
 59. Kugel K I, Rakhmanov A L, Sboychakov A O, Poccia N, and Bianconi A, 2008 *Phys. Rev. B* 78, 165124.
 60. Siegel D A *et al.* 2011 *Proc. Nat. Acad. Scie.* 108, 11365.
 61. Smallwood C L *et al.* 2012 *Science* 336, 1137.
 62. Fratini M *et al.* 2010 *Nature* 466, 841.
 63. Poccia N *et al.* 2012 *Proc. Nat. Acad. Scie.* 109, 15685.
 64. Poccia N *et al.* 2013 *J. Supercond. Nov. Magn.* 26, 2703-2708.
 65. Ricci *et al.* 2013 *Scie. Rep.* 3, 238.
 66. Campi G *et al.* 2013 *Phys. Rev. B* 87, 014517.
 67. Geballe T H, and Marezio M, 2009 *Phys. C: Supercond.* 469, 680-684.
 68. Zeljkovic I *et al.* 2012 *Science* 337, 320.
 69. Jarlborg T, and Bianconi A, 2013 *Phys. Rev. B* 87, 054514.
 70. Flank A M *et al.* 2006 *Nucl. Instrum. Meth., Phys. Res. Sect. B* 246, 269.
 71. Jorgensen D *et al.* 1988 *Phys. Rev. B* 38, 11337.
 72. Chaillout C *et al.* 1990 *Phys. C: Supercond.* 170, 97.
 73. Radaelli P *et al.* 1994 *Phys. Rev. B* 49, 6239.
 74. Wells B *et al.* 1996 *Z. Phys. B* 100, 535
 75. Wells B *et al.* 1997 *Science* 277, 1067.
 76. Radaelli P *et al.* 1993 *Phys. Rev. B* 48, 499.
 77. A. Lanzara *et al.* 1997 *Phys. Rev. B* 55, 9120
 78. Di Castro D *et al.* 2000 *Europ. Phys. J. B-Cond. Matty. Com. Sys* 18, 617-624.
 79. Poccia N and Fratini M 2009 *J. Supercond. Nov. Magn.* 22, 299-303.
 80. Poccia N, Ricci A and Bianconi A 2010 *Adv. Cond. Matt. Phys.* 2010, 261849.
 81. Agrestini S *et al.* 2014 *J. Phys. Chem. Solids* 75, 259-264.
 82. Hor P. *et al* 1996 *J. Phys. Chem. Solids* 57, 1061.